Effects of Processing Parameters on the Microstructures and Mechanical Properties of *In Situ* ($Al_3Ti + Al_2O_3$)/Al Composites Fabricated by Hot Pressing and Subsequent Friction-Stir Processing

Q. ZHANG, B.L. XIAO, Q.Z. WANG, and Z.Y. MA

In situ ($Al_3Ti + Al_2O_3$)/Al composites were fabricated in an Al-TiO_2 system by the combination of hot pressing (HP) and friction-stir processing (FSP). The effects of HP and FSP parameters on the microstructures and mechanical properties of the *in situ* composites were studied. The Al-TiO_2 reaction extent increased with increasing the temperature and holding time of HP. Subsequent FSP not only induced Al-TiO_2 reaction, resulting in the formation of nanosized Al_3Ti and Al_2O_3, but also rounded the polygonal Al_3Ti particles formed during HP. The tensile strength of the FSP sample in which the Al-TiO_2 reaction took place completely during HP was lower than that of the FSP samples in which the Al-TiO_2 reaction took place hardly or partly during HP. For the FSP samples in which the Al-TiO_2 reaction took place hardly during HP, the volume fraction of reinforcing particles increased with decreasing the traverse speed, resulting in the increase in tensile strength of the FSP samples. At a traverse speed of 25 mm/min, increasing the rotation rate from 1000 to 2000 rpm produced little influence on the microstructures and mechanical properties of the *in situ* composites. Additional 2-pass FSP in water refined the matrix grains, resulting in the significant increase in the tensile strength.

DOI: 10.1007/s11661-014-2221-5

I. INTRODUCTION

FRICTION-STIR processing (FSP), a development based on friction-stir welding (FSW), is a solid-state processing technique for microstructure modification.[1] During FSP, the material in the stir zone (SZ) undergoes intense plastic deformation, mixing and thermal exposure, leading to significant microstructural changes. Recently, it was reported that FSP could induce reaction between Al and suitable metals or metal oxides, such as Ti, Cu, TiO_2, *etc.*, to produce *in situ* Al matrix composites (AMCs) with a good combination of strength and ductility.[2–6] The occurrence of *in situ* reaction during FSP can be attributed to the enhanced solid diffusion and the mechanically activated effect caused by severe deformation of FSP.[5,6]

Generally, before FSP is run for fabricating *in situ* AMCs, the conventional hot pressing (HP) or sintering route was used to form a precursor from a powder mixture of constituents.[2–7] The main purpose of HP or sintering is to produce a billet with enough strength and ductility for subsequent FSP. However, depending upon the parameters of HP or sintering, different extents of *in situ* reaction might occur during HP or sintering, and this exerted significant influence on the microstructure evolution during subsequent FSP and the mechanical properties of the resultant composites because the size and morphology of reinforcing particles formed during HP or sintering and FSP may be different due to different formation mechanisms. For example, in a previous study,[7] we investigated the mechanical properties of *in situ* Al_3Ti/Al composites fabricated by HP and subsequent FSP, and we found that the sample with complete Al-Ti reaction during HP and a subsequent FSP at a tool rotation rate of 1000 rpm exhibited an optimal combination of strength and ductility.

Furthermore, FSP parameters, such as the tool rotation rate, traverse speed, and cooling condition (natural cooling in air or cooling by flowing gas or liquid, *etc.*) during FSP, would influence plastic deformation and thermal cycle in the SZ, and therefore, would change the microstructures and mechanical properties of FSP AMCs. Chen *et al.*[8] fabricated the *in situ* composites in the Al-CeO_2 system by FSP and studied the effect of the tool traverse speed on the microstructures and mechanical properties of the composites. It was reported that the sample produced at a higher tool traverse speed of 120 mm/min exhibited lower strength than those produced at lower tool traverse speeds of 30 and 85 mm/min, which was attributed to the lower content of reinforcing particles produced at the higher tool traverse speed due to the

Q. ZHANG, formerly Postgraduate with the Shenyang National Laboratory for Materials Science, Institute of Metal Research, Chinese Academy of Sciences, 72 Wenhua Road, Shenyang 110016, P.R. China, is now Engineer with the CHINALCO Research Institute of Science and Technology, No. 62, Xizhimen North Street, Haidian District, Beijing 100082, P.R. China. B.L. XIAO and Z.Y. MA, Professors, and Q.Z. WANG, Associate Professor, are with the Shenyang National Laboratory for Materials Science, Institute of Metal Research, Chinese Academy of Sciences. Contact e-mail: zyma@imr.ac.cn

Manuscript submitted June 7, 2013.
Article published online February 19, 2014

shorter reactive time and lower reactive temperature. However, because the heat release of the thermite reaction between Al and CeO_2 was severe, FSP had to be conducted at a low tool rotation rate of 500 rpm to obtain defect-free samples, and the effect of tool rotation rate on the *in situ* composites was not studied. Recently, the current authors[9] reported that additional 2-pass FSP with rapid water cooling produced ultrafine matrix grains with a high density of dislocations in the *in situ* Al_3Ti/Al composites, leading to the significant increase in the strength of the composites.

In a recent study, we reported some results about the mechanical properties and reactive mechanism of *in situ* (Al_3Ti + Al_2O_3)/Al composites fabricated by HP and subsequent FSP from the Al-TiO_2 system.[6] It was shown that the *in situ* (Al_3Ti + Al_2O_3)/Al composites exhibited the good combination of strength and ductility, and the formation mechanisms of Al_3Ti and Al_2O_3 were deformation-assisted solution-precipitation and deformation-assisted interfacial reaction, respectively. However, the *in situ* composite was fabricated only using a set of processing parameters,[6] and the effect of the FSP parameters is still lacking.

In the current study, a wide range of HP and FSP parameters, including the temperature and holding time of HP and the tool rotation rate, traverse speed, and active cooling (accelerate the cooling rate of SZ by flowing water) of FSP, were employed to fabricate the *in situ* (Al_3Ti + Al_2O_3)/Al composites in the Al-TiO_2 system. Our preliminary study also indicated defect-free SZ could be obtained under the current designed parameters, while beyond these parameters, some defects would form easily in the SZ during FSP. The aim of this study is to establish the relationship among the fabricating parameters, microstructure, and mechanical properties of the *in situ* (Al_3Ti + Al_2O_3)/Al composites.

II. EXPERIMENTAL

The starting materials used were commercial pure Al powder (99.9 pct purity, 13 μm) and rutile TiO_2 powders (99 pct purity, 150 nm). The volume fractions of Al_3Ti and Al_2O_3 particles were amounted to 15 pct, assuming that the reaction takes place completely to form Al_3Ti and Al_2O_3. The Al and TiO_2 powders were mixed in a biaxis rotary mixer with a rotation rate of 50 rpm for 12 hours and then cold compacted into billets. The cold-compacted billets were heated to the designed temperature in a vacuum furnace and then hot pressed after held for a period of time. The temperature and holding time of HP for various billets are shown in Table I. The HP billets were 60 mm in diameter and 80 mm in height (illustrated by Figure 1(a)). To improve the ductility of the HP billets and obtain the enough size for the subsequent FSP, the HP billets were free forged in an open die using 200 MPa pressure at 753 K (480 °C). The total deformation ratio was 4:1. The forged plates are cylindrical shaped with a diameter of 120 mm and a height of 20 mm (illustrated by Figure 1(b)).

The forged plates were subjected to 4-pass FSP with 100 pct overlapping (illustrated by Figure 1(c)). A cermet tool with a concave shoulder 20 mm in diameter, a threaded cylindrical pin 6 mm in diameter, and 5 mm in length was used. The FSP parameters used in this study were also summarized in Table I. As shown in Table I, except for sample 8, the FSP runs of all the other samples were conducted in air. For sample 8, the first four FSP passes were carried out at a traverse speed of 25 mm/min in air and the final two FSP passes were carried out at 50 mm/min in the flowing water to increase the cooling rate during FSP. The details about water cooling had been described in our previous study.[4]

The samples for microstructural investigations were cut in the SZ in the transverse direction to the FSP. The location of microstructural investigation is shown in Figure 1(d). The microstructures were examined by scanning electron microscopy (SEM; Quanta 600; FEI Corporation, Hillsboro, OR) complemented by energy-dispersive X-ray spectroscopy (EDS), and transmission electron microscopy (TEM; TECNAI20; FEI Corporation). An X-ray diffraction analyzer (D/max 2400; Rigaku Corporation, Tokyo, Japan) was used to

Table I. HP and FSP Parameters Used in this Study

	HP		FSP		
Sample	Temperature [K (°C)]	Holding Time (min)	Rotation Rate (rpm)	Traverse Speed (mm/min)	FSP Pass
1	773 (500)	5	1000	25	4
2	823 (550)	50	1000	25	4
3	903 (630)	240	1000	25	4
4	773 (500)	5	1000	100	4
5	773 (500)	5	1000	50	4
6(1)*	773 (500)	5	1000	25	4
7	773 (500)	5	2000	25	4
8	773 (500)	5	1000	25/50	6**

*The fabricating parameters of samples 6 and 1 were the same. Samples 1–3 were used to investigate the influence of HP parameters, while samples 4–8 were used to investigate the influence of FSP parameters.

**The first four FSP passes were carried out at a travel speed of 25 mm/min, and the final two FSP passes were carried out at 50 mm/min in flowing water.

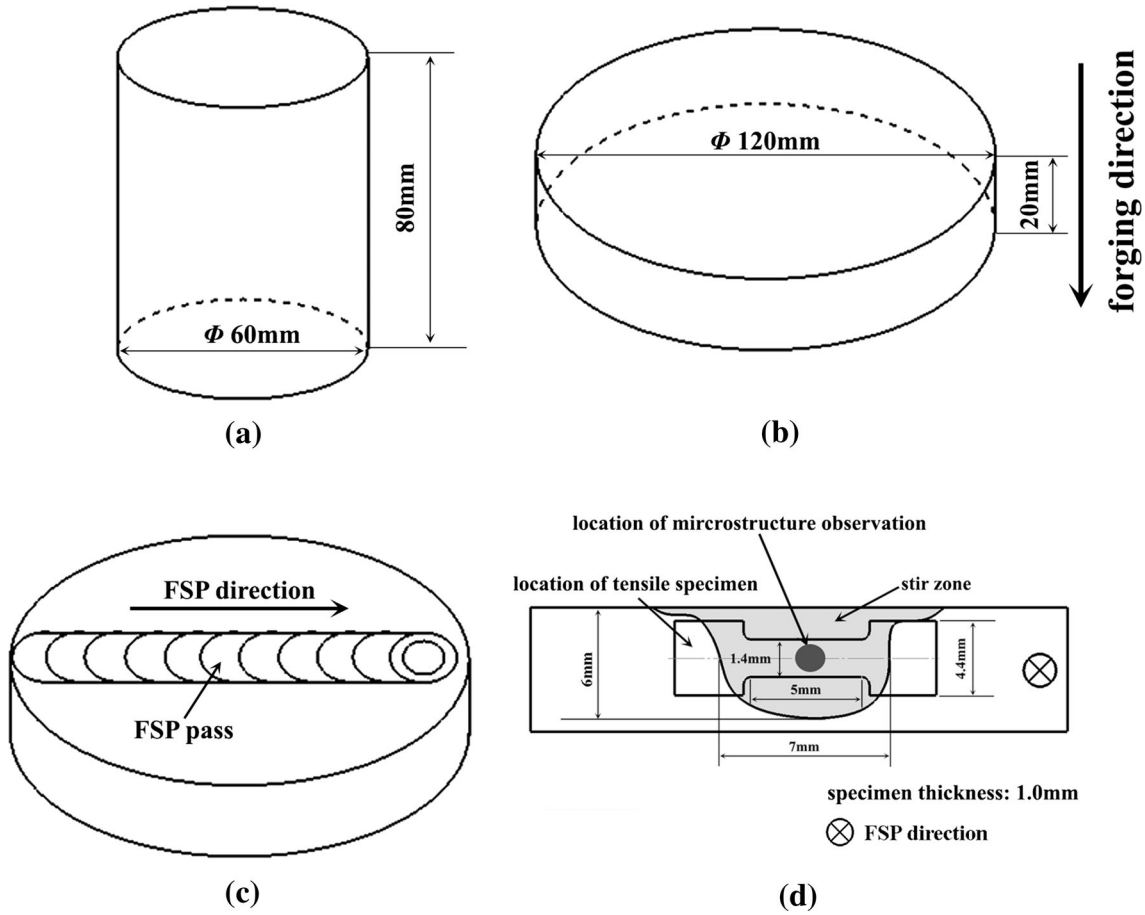

Fig. 1—Schematic illustrations of (*a*) HP billet, (*b*) forged billet, (*c*) FSP run, and (*d*) locations of microstructure observation and tensile specimen.

identify the phases of the composites. Thin foils for TEM were prepared by the ion-milling technique.

Dogbone-shaped tensile specimens (5.0 mm gage length, 1.4 mm gage width, and 1.0 mm gage thickness) were electrical discharge machined from the SZ, transverse to the FSP direction, as shown in Figure 1(d). Tensile tests were conducted using an INSTRON 5848 microtester (Instron Corporation, Norwood, MA) at an initial strain rate of 1×10^{-3} second^{-1}. The property values for each condition were calculated by averaging three test results. After the tensile test, the fracture surfaces were examined using SEM.

III. RESULTS AND DISCUSSION

A. *Microstructure*

1. *Effects of HP parameters*

Figure 2 shows the X-ray diffraction (XRD) patterns of forged samples 1 – 3. For sample 1, no evident peaks except for Al and TiO_2 peaks were detected, indicating that almost no reaction between Al and TiO_2 took place during HP and forging. For sample 2, the intensity of TiO_2 peaks decreased compared with that in sample 1,

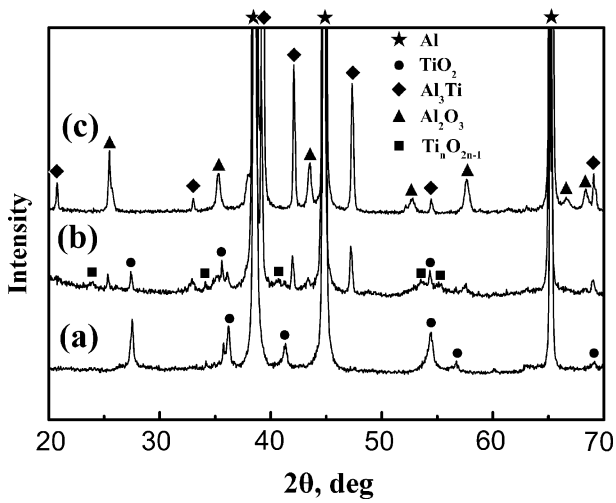

Fig. 2—XRD patterns of forged samples 1 – 3: (*a*) sample 1, (*b*) sample 2 and (*c*) sample 3.

whereas the peaks of Al_3Ti and Al_2O_3 became evident. Meanwhile, some oxygen-deficient titanium oxides (formulized as Ti_nO_{2n-1}, such as Ti_2O_3 or TiO) were revealed. These results indicated that partial reaction

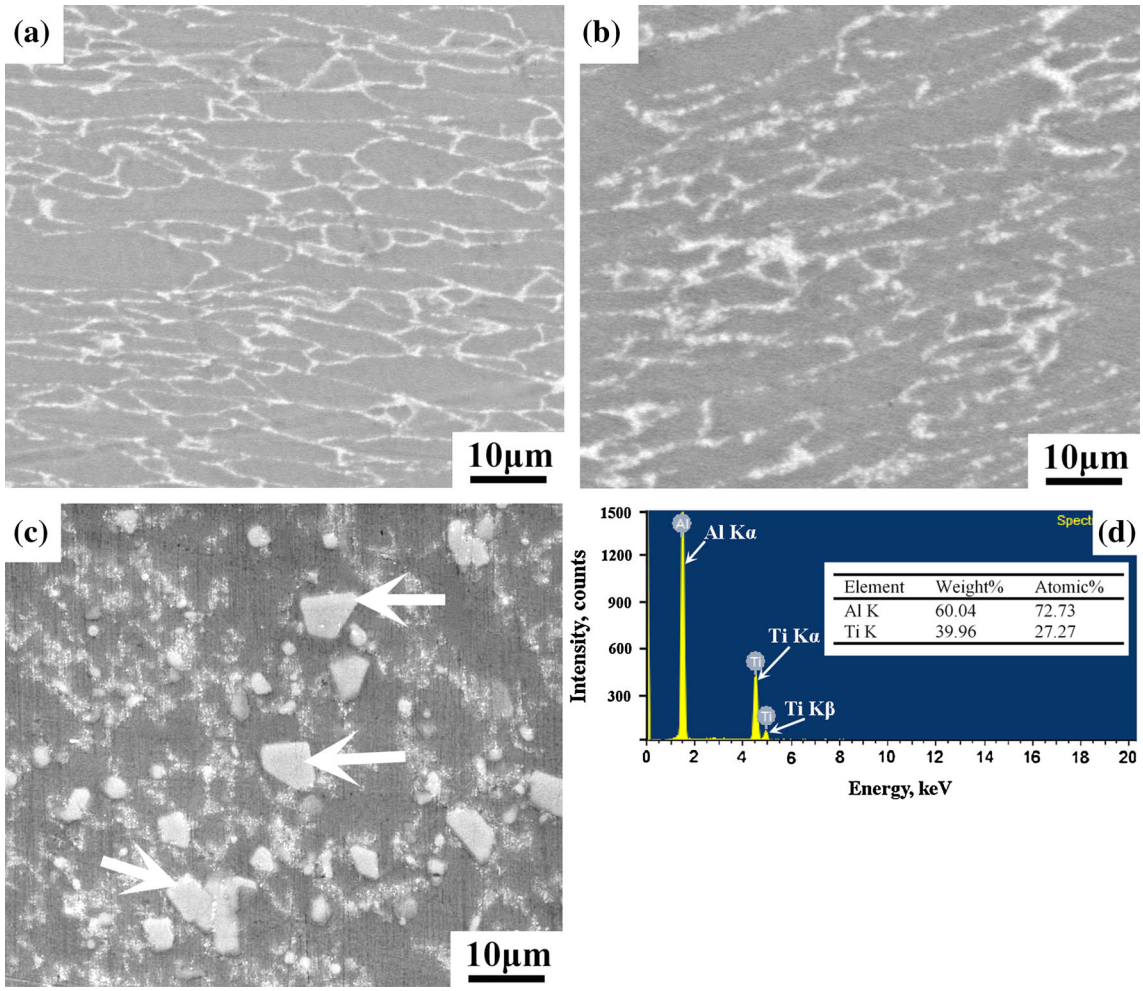

Fig. 3—SEM images of forged samples 1 – 3: (*a*) sample 1, (*b*) sample 2, (*c*) sample 3, and (*d*) EDS of polygonal particles in sample 3.

between Al and TiO_2 took place after HP at 823 K (550 °C) for 50 minutes. For sample 3, the peaks corresponding TiO_2 and Ti_nO_{2n-1} all disappeared, and only Al, Al_3Ti, and Al_2O_3 peaks were detected, indicating that after HP at 903 K (630 °C) for 240 minutes, all TiO_2 reacted with Al to form Al_3Ti and Al_2O_3.

Figure 3 shows the SEM images of forged samples 1 – 3. In sample 1, some particles were distributed as chains at the elongated Al particle boundaries due to the large particle size ratio of aluminum particles to reinforcing particles (PSR) (Figure 3(a)). For particle-reinforced aluminum matrix composites fabricated by the powder metallurgy technique, when the PSR is 1, the reinforcing particles would be distributed homogeneously in the matrix, and when the PSR is greater than 1, the reinforcing particles would be distributed as chains at the boundaries of the initial aluminum particles.[10] In sample 2, the distribution of particles did not change; however, the particle distribution chains were broadened (Figure 3(b)). In sample 3, some coarse particles with a polygonal shape were found near the initial particle distribution chains where some fine particles could still be observed (Figure 3(c)). The coarse particles with a polygonal shape were identified as Al_3Ti by EDS (Figure 3(d)).

Figure 4 shows the TEM images of forged samples 2 and 3. In sample 2, some Al_3Ti with a size of about 100 nm and partially reacted TiO_2 could be observed in the particle distribution chains (Figure 4(a)). In sample 3, the fine particles with a size of about 150 nm in the particle distribution chains were identified as Al_2O_3 by selected-area electron diffraction patterns (Figure 4(b)).

Because the temperatures of HP in the current study were all lower than the melting point of Al (933 K [660 °C]), the reaction between Al and TiO_2 could be classified as a solid-state diffusion reaction. Schaffer and McCormick[11] suggested that the solid-state reaction rate was controlled by diffusion of the reactants through the product materials. The reaction was therefore dependent on the initial contact area, particles size, local temperature, *etc*. For sample 1, the HP temperature was relatively lower and the holding time during HP was shorter; thus, the Al-TiO_2 reaction did not take place almost. With increasing the temperature and extending the holding time of HP, the Al-TiO_2 reaction started to take place. The Al-TiO_2 reaction can be

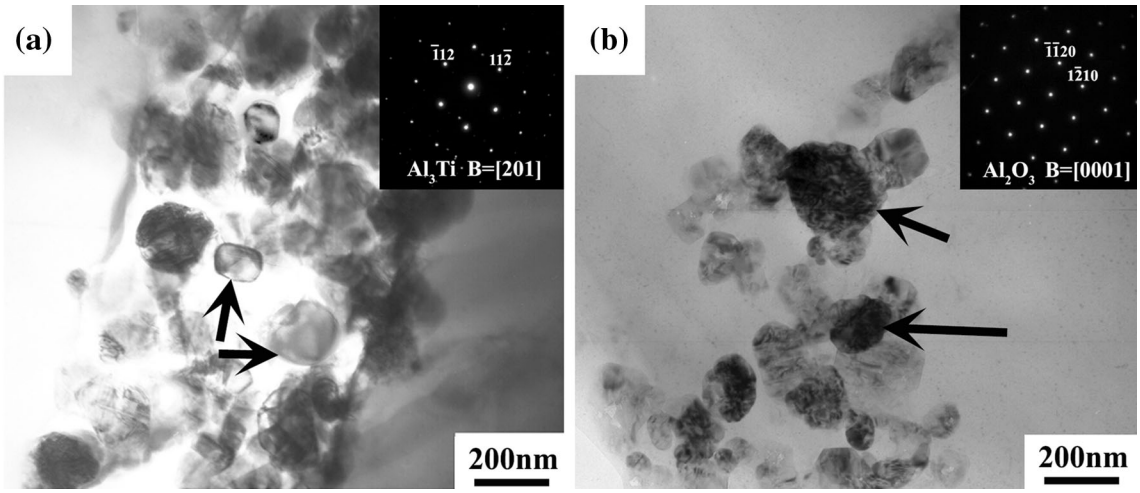

Fig. 4—TEM images of forged (*a*) sample 2 and (*b*) sample 3.

divided into two steps: First, TiO_2 reacts with Al to form Al_2O_3 and free Ti atoms; second, the displaced Ti atoms react with Al to form Al_3Ti.[12] The reaction formulas are as follows:

$$3TiO_2 + 4Al \rightarrow 2\alpha - Al_2O_3 + 3[Ti] \quad [1]$$

$$[Ti] + 3Al \rightarrow Al_3Ti \quad [2]$$

In the HP samples, TiO_2 particles aggregated at the initial Al particle boundaries (Figure 2(a)). The reaction was controlled by solid-state diffusion at point contacts, and Al_2O_3 would form at the contact points.[6] As the reaction proceeded, a TiO_2 particle gradually transformed into one or two Al_2O_3 particles from the contact points. So in forged sample 3 in which the Al-TiO_2 reaction took place completely, Al_2O_3 particles with sizes similar to the initial TiO_2 powders formed at the locations of initial particle distribution chains.

The results of Feng and Froyen[13,14] and our previous study[6] suggested that some oxygen-deficient titanium oxides (Ti_nO_{2n-1}), such as Ti_2O_3 or TiO, were formed as intermediate products during the reaction between Al and TiO_2 (Reaction 1). In the current study, some peaks corresponding to Ti_nO_{2n-1} were also observed in forged sample 2 because of an incomplete reaction between Al and TiO_2. And in sample 3 hot pressed at 903 K (630 °C) for 240 minutes, all the TiO_2 and Ti_nO_{2n-1} reacted with Al to form the final products Al_2O_3 and Al_3Ti.

According to Eq. [1], some free Ti atoms would be reduced from TiO_2. Because Ti has low diffusivity and solubility in solid-state Al,[15] Al_3Ti would form near the Al-TiO_2 reactive interface. In forged sample 2, the size of Al_3Ti was fine for the following reasons. First, only partial TiO_2 reacted with Al in sample 2, resulting in the low concentration of free Ti atoms in Al. Second, the HP temperature was still lower and the holding time was shorter for sample 2. For forged sample 3, a large number of Ti atoms was available due to the complete reaction between Al and TiO_2 during HP at 903 K (630 °C) for 240 minutes, so more Al_3Ti formed and grew into coarse particles near the Al-TiO_2 reactive interface.

In the previous studies, Ma and Tjong[12] and Zhu *et al.*[16] also fabricated *in situ* ($Al_3Ti + Al_2O_3$)/Al composites in Al-TiO_2 system by HP. However, the Al_3Ti particles in these two studies were rod shaped with a large aspect ratio. In the current study, the Al_3Ti particles were polygonal and the aspect ratio was relatively low (Figure 3(c)). This may be attributed to the different HP temperatures in the previous and the current studies. In the studies by Ma and Tjong[12] and Zhu *et al.*,[16] the HP temperature was 1073 K (800 °C), which was above the melting point of Al (933 K [660 °C]). Free Ti atoms reduced from TiO_2 would first dissolve into molten Al at 1073 K (800 °C), and then precipitate as Al_3Ti during the cooling.[12] In this case, Al_3Ti would grow into the rod shape along a special orientation in the molten Al. In the current study, the HP temperature was below the melting point of Al. Because Ti has low diffusivity and solubility in solid-state Al,[15] Ti atoms could not be diffused far away from reactive interface, and Al_3Ti would be formed and gradually grew to coarse particles with a small aspect ratio near the reactive interface during the isothermal holding of HP.

Figure 5 shows the XRD patterns of FSP samples 1 – 3. It can be seen that, except for the peaks of Al, Al_3Ti, and Al_2O_3, no other peaks were detected in these three samples. This indicated that all the TiO_2 and Ti_nO_{2n-1} in forged samples 1 and 2 reacted with Al to form Al_3Ti and Al_2O_3 during FSP.

Figure 6 shows the SEM images of FSP samples 1 – 3. In the three FSP samples, the initial Al particle boundaries disappeared completely and the reinforcing particles were distributed homogeneously. In FSP samples 1 and 2, the reinforcing particles were too fine to be resolved under SEM. In FSP sample 3, most of Al_3Ti particles changed from polygon to rounded shape, and some fine Al_3Ti particles were also observed.

Figure 7 shows the TEM images of FSP samples 1 – 3. In FSP samples 1 and 2, some equiaxed particles with a size of about 100 nm were observed. Based on our previous study[6] and the XRD patterns in Figure 5, these equiaxed particles were Al_3Ti and Al_2O_3. Furthermore, some floc-shaped particles were also revealed in FSP samples 1 and 2, and they were the intermediate products of Al-TiO_2 reaction composed of some oxygen-deficient titanium oxides, based on our previous study.[6] In FSP sample 3, the number of nanosized particles decreased compared with that in FSP samples 1 and 2, and these particles with a size of about 150 nm were identified as Al_2O_3 by selected-area electron diffraction patterns.

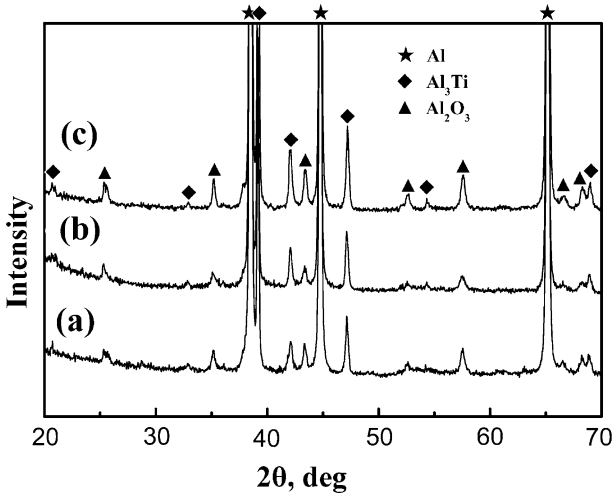

Fig. 5—XRD patterns of FSP samples 1 – 3: (a) sample 1, (b) sample 2, and (c) sample 3.

Previous studies[5,6] suggested that severe plastic deformation during FSP would enhance the solid diffusion and decrease the reactive activation energy, thereby inducing the Al-TiO_2 reaction to form Al_3Ti and Al_2O_3 particles in the matrix. The formation mechanisms of Al_3Ti and Al_2O_3 were determined to be deformation-assisted solution-precipitation and interfacial reaction, respectively.[6] The Al_3Ti and Al_2O_3 particles formed during FSP were generally nanosized due to the special formation mechanisms.

In the current study, Al_3Ti and Al_2O_3 particles in FSP sample 1 were formed during FSP; thus, their size was fine (~ 100 nm). For sample 2, although a partial Al-TiO_2 reaction had taken place during HP and

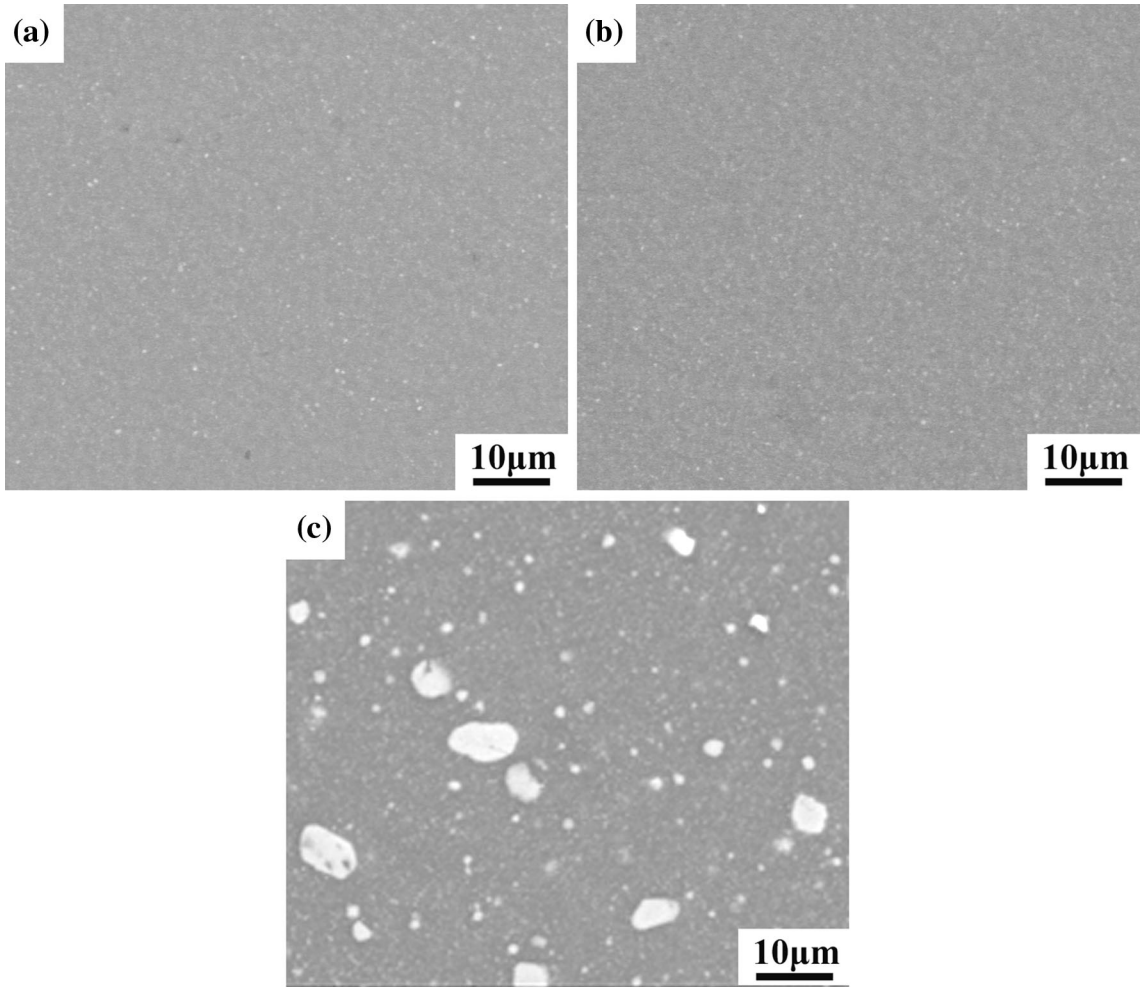

Fig. 6—SEM images of FSP samples 1 – 3: (*a*) sample 1, (*b*) sample 2, and (*c*) sample 3.

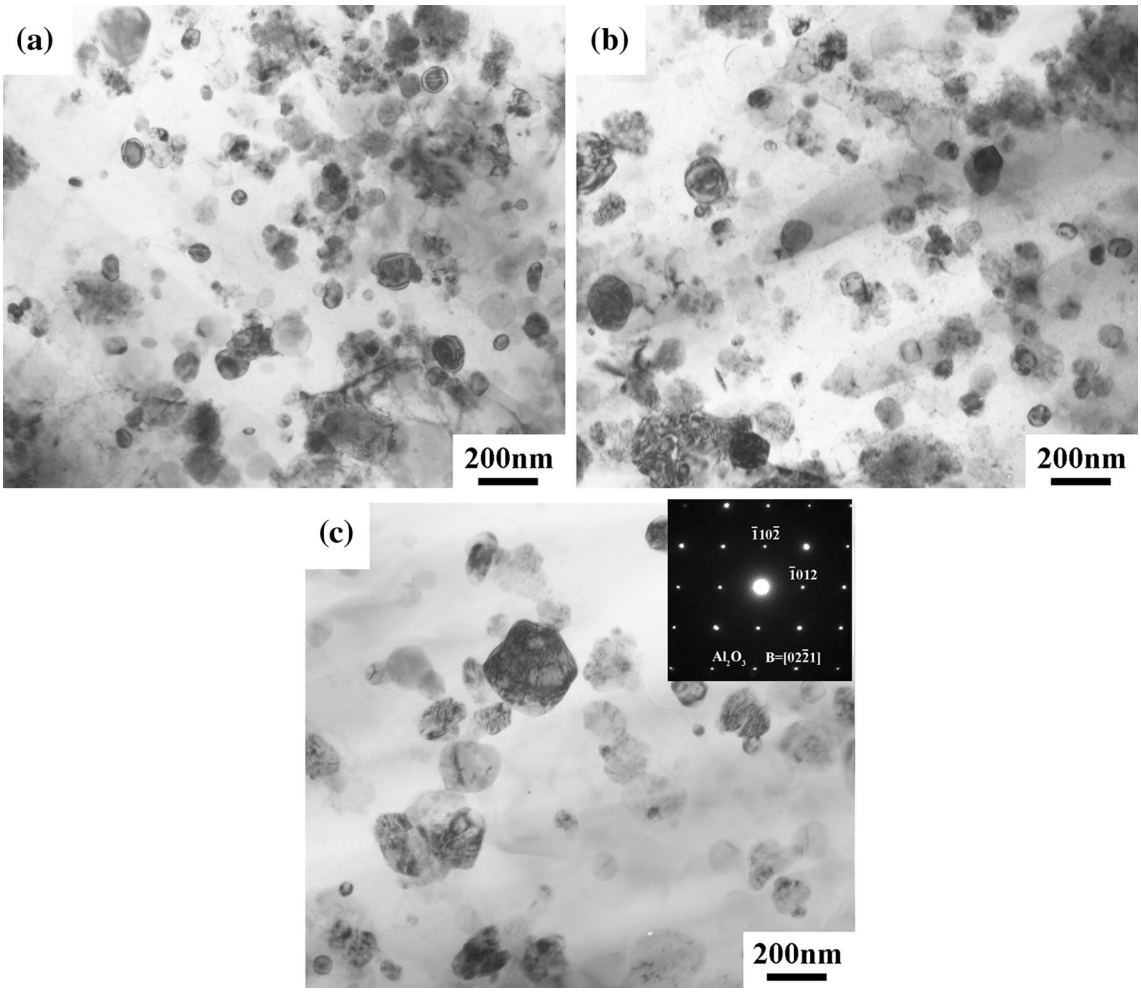

Fig. 7—TEM images of FSP samples 1 – 3: (*a*) sample 1, (*b*) sample 2, and (*c*) sample 3.

forging, the size of Al_3Ti in the forged sample was still fine (~ 100 nm) due to the relatively low temperature and short holding time of HP. During the subsequent FSP, the remaining TiO_2 reacted with Al to form nanosized Al_2O_3 and Al_3Ti, and the Al_3Ti particles formed in HP did not coarsen obviously during FSP due to the short duration of thermal exposure and good thermal stability of Al_3Ti.[15] For sample 3, all TiO_2 had reacted with Al to form Al_2O_3 with a size of about 150 nm and coarse Al_3Ti particles with a polygonal shape during HP. During the subsequent FSP, Al_2O_3 particles were distributed in the matrix homogeneously; at the same time, the edges and corners of most of polygonal Al_3Ti were rounded, creating some small Al_3Ti particles in the matrix.

According to the previous studies,[17–19] the refining of second-phase particles in the Al matrix during FSP/FSW depends on not only the tool geometry and processing parameters of FSP/FSW but also on the stiffness, ductility, initial size, and aspect ratio of the particles; the strength of the matrix; and so on. For example, Ma *et al.*[17] suggested that FSP would significantly break up the acicular Si particles in cast A356 alloy. However, for Al_2O_3 or SiC particle-reinforced aluminum alloy matrix composites,[18,19] FSP/FSW did not exert obvious influence on the size of the reinforcing particles but blunted the edges and the corners of the particles.

In our previous study[7] about *in situ* Al_3Ti/Al composites fabricated by the combination of HP and FSP, FSP could significantly refine the A_3Ti particles formed during HP. However, the coarse Al_3Ti particles in Reference 7 were formed through reactive diffusion between Ti and Al particles during HP, and additional stress caused by the formation of Al_3Ti would introduce some microcracks in the Al_3Ti particles. So the Al_3Ti particles were broken up easily during the subsequent FSP. In the current study, however, the Al_3Ti particles were formed due to a reaction between free Ti atoms and Al and grew gradually to coarse particles with a small aspect ratio during isothermal holding of HP. In this case, no microcracks would form in the Al_3Ti particles (Figure 3(c)). Therefore, during the subsequent FSP, the refinement of Al_3Ti was not obvious and most of Al_3Ti were just rounded, like the situation of SiC or Al_2O_3 particles during FSW of SiC or Al_2O_3 particle-reinforced Al composites.[18,19]

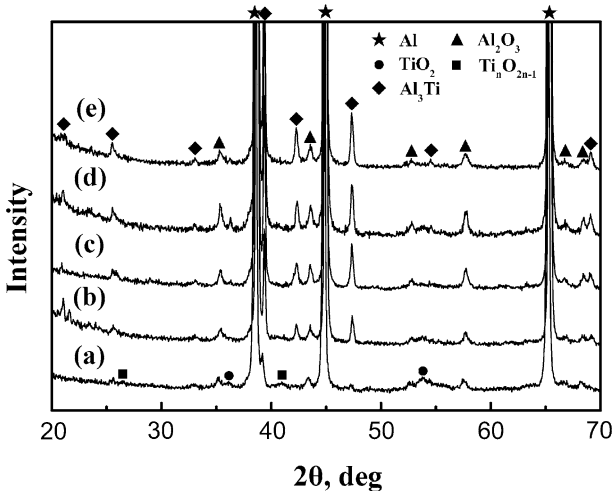

Fig. 8—XRD patterns of FSP samples 4 – 8: (a) sample 4, (b) sample 5, (c) sample 6, (d) sample 7, and (e) sample 8.

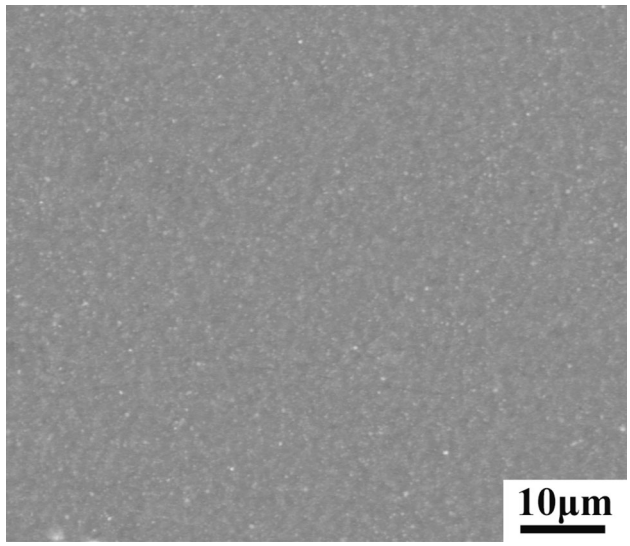

Fig. 9—SEM images of FSP sample 4.

2. *Effect of FSP parameters*

Figure 8 shows the XRD patterns of FSP samples 4 – 8. The HP temperatures of samples 4 – 8 were 773 K (500 °C), which was the same as that of sample 1, so TiO_2 would not react with Al during HP. After 4-pass FSP at a tool rotation rate of 1000 rpm and a traverse speed of 100 mm/min (sample 4), the peaks corresponding to TiO_2 became weak, and some weak peaks of Al_3Ti, Al_2O_3 and Ti_nO_{2n-1} were observed. When the traverse speed decreased to 50 mm/min (sample 5), the peaks of TiO_2 and Ti_nO_{2n-1} disappeared and the peaks of Al_3Ti and Al_2O_3 became evident. The intensity of Al_3Ti and Al_2O_3 peaks increased further when the traverse speed decreased to 25 mm/min (sample 6). At a traverse speed of 25 mm/min, increasing the tool rotation from 1000 to 2000 rpm caused little influence on the XRD patterns of samples (sample 7). Furthermore, additional 2-pass FSP in water after 4-pass FSP in air also exerted little influence on the XRD patterns of samples (sample 8).

Figure 9 shows the SEM image of FSP sample 4. After FSP, the initial Al particle boundaries disappeared completely, and the reinforcing particles were too fine to be resolved under SEM. The SEM images of FSP samples 5 – 8 exhibit similar characteristics with that of FSP sample 4 (not shown).

Figure 10 shows the TEM images of FSP samples 4 – 7. In FSP sample 4, numerous floc-shaped particles were observed, and only a small number of equiaxed particles with the size less than 20 nm were found. Because the traverse speed of FSP sample 4 was 100 mm/min, the relatively high traverse speed caused lower temperature and smaller strain in the SZ, and the duration of FSP was very short. Thus, only partial Al-TiO_2 reaction took place during FSP, resulting in the formation of some floc-shaped particles, which is the intermediate reactive products of Al-TiO_2 reaction, and a small number of Al_2O_3 and Al_3Ti particles.

From Figures 10(a) – (c), it can be seen that the number of equiaxed particles increased with decreasing the traverse speed from 100 to 25 mm/min. Decreasing the traverse speed from 100 to 25 mm/min caused higher temperature and more severe deformation in the SZ, resulting in greater diffusion enhancement and mechanical activation effect. Thus, more TiO_2 reacted with Al to form Al_2O_3 and Al_3Ti. Furthermore, because Al_3Ti and Al_2O_3 have the low coarsening rate at about 873 K (600 °C),[15] the size of Al_3Ti and Al_2O_3 was still about 100 nm even when the traverse speed decreased to 25 mm/min.

At the traverse speed of 25 mm/min, increasing the tool rotation rate from 1000 to 2000 rpm caused little influence on the size and number of equiaxed particles (Figures 10(c) and (d)). Furthermore, little difference was found between the XRD patterns of FSP samples at rotation rate of 1000 and 2000 rpm (Figure 8). These results suggested increasing the tool rotation rate from 1000 to 2000 rpm exerted little influence on the *in situ* Al-TiO_2 reaction during FSP.

As mentioned above, the *in situ* reaction can be significantly enhanced by severe deformation of FSP. However, the results of our previous study[5] indicated that there was a limit for the enhancement of *in situ* reaction by FSP beyond which intensifying deformation exerted little effect on the reaction, and FSP with a rotation rate of 1000 rpm may be close to this limit for the Al-Ti reaction. The fact that increasing the tool rotation rate from 1000 to 2000 rpm exerted little influence on the *in situ* Al-TiO_2 reaction again verified this viewpoint. A similar result was also reported recently about *in situ* Al-SiO_2 reaction during FSP by You *et al.*[20]

Figure 11 shows the grain microstructure of FSP samples 4 – 7. Generally, the grain boundaries of *in situ* Al composites were not easily distinguished completely. However, the matrix grain size in the FSP samples at different FSP parameter combinations was estimated to be on the order of ~1.5 – 2 μm, indicating that changing

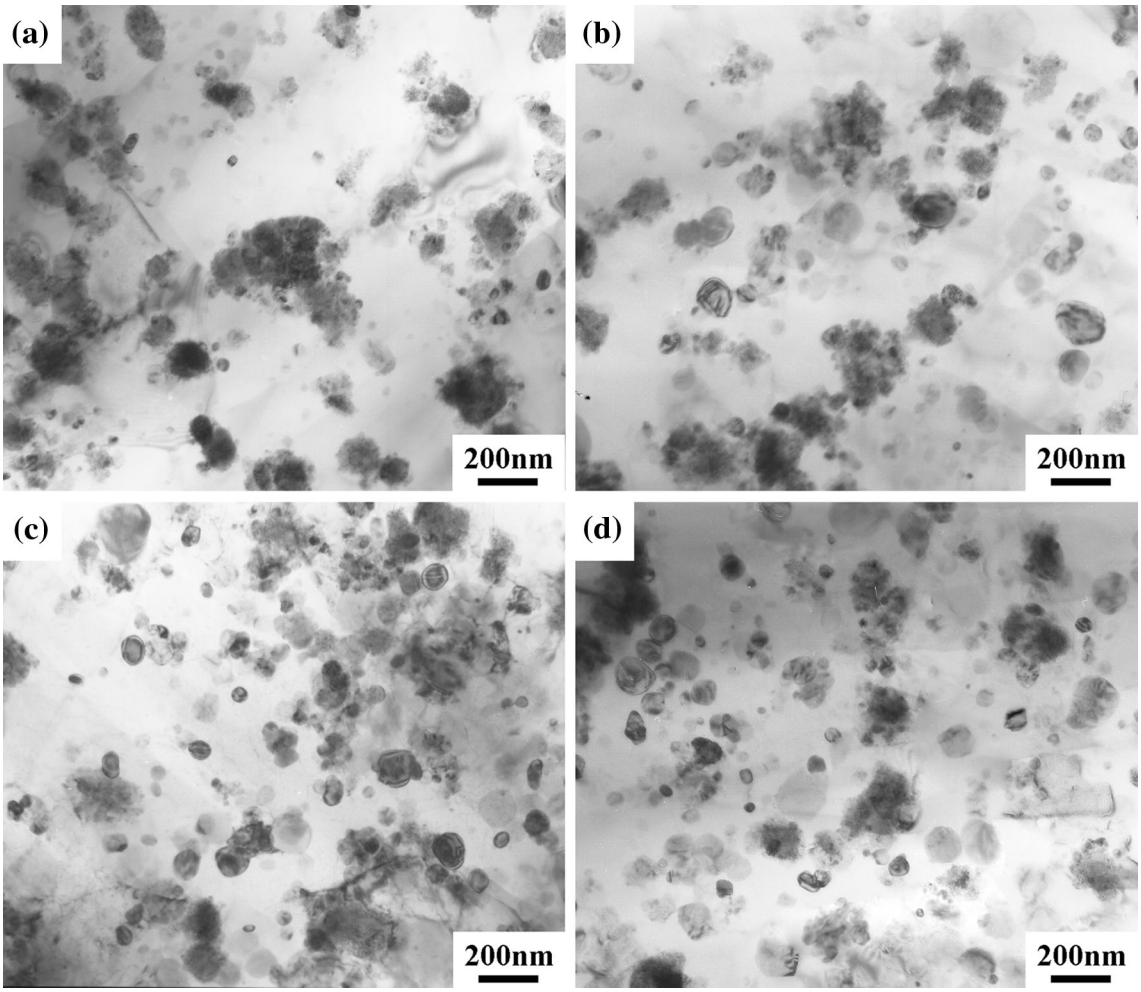

Fig. 10—TEM images of FSP samples 4 – 7 showing the reinforcing particles in (*a*) sample 4, (*b*) sample 5, (*c*) sample 6, and (*d*) sample 7.

FSP parameters had no detectable effect on the matrix grain size of the *in situ* composites.

Generally, FSP results in the fine and equiaxed grains in the processed samples due to dynamic recrystallization.[21] Therefore, the factors influencing the nucleation and growth of the dynamic recrystallization would determine the resultant grain microstructure of FSP samples. For Al alloys, increasing the tool rotation rate or the tool rotation-rate/traverse-speed ratio, which introduces higher heat input during FSP, would result in the coarser grains.[21–23] However, for the nanoparticle-reinforced metal matrix composites, the grain microstructures of the FSP samples are influenced not only by the heat input during FSP but also by the reinforcing nanoparticles. The nanoparticles would pin the grain boundaries and then inhibit the growth of the recrystallized grains.[24]

For sample 4, although higher traverse speed introduced lower heat input during FSP, it also resulted in the formation of less Al_3Ti and Al_2O_3. The inhibition effect of the particles would be relatively weak. Decreasing the traverse speed introduced higher heat input during FSP; however, it also resulted in the formation of more Al_3Ti and Al_2O_3. The combined effect of heat input and pining effect of nanoparticles resulted in that decreasing the traverse speed did not exert obvious influence on the matrix grain size of the *in situ* composites. Similar results were reported by Ma *et al.*[25] in FSP A356 alloy and by You *et al.*[20] in *in situ* nano-Al_2O_3 reinforced Al composites fabricated from Al-SiO_2 system by FSP.

For the particle-reinforced metal matrix composites, it is known that the grain growth would stop when the matrix grain size achieves the limiting value (d_z). d_z is related to the volume fraction and size of reinforcing particles, as shown in Eq. [3].[26]

$$d_z = \frac{\mathrm{k}r}{f^n} \qquad [3]$$

where r and f is the radius and volume fraction of reinforcing particles, respectively, k is a dimensionless constant, and n varies between 0.33 and 1. For the composites containing volume fractions of particles less than 5 pct, the values of limiting size calculated by Eq. [3] were in good agreement with the experimental values.[24] However, for the composite containing a large volume fraction of particles, the experimental measurements of limiting grain size were scattered.[24] Nevertheless, the previous results[24] indicated that the limiting

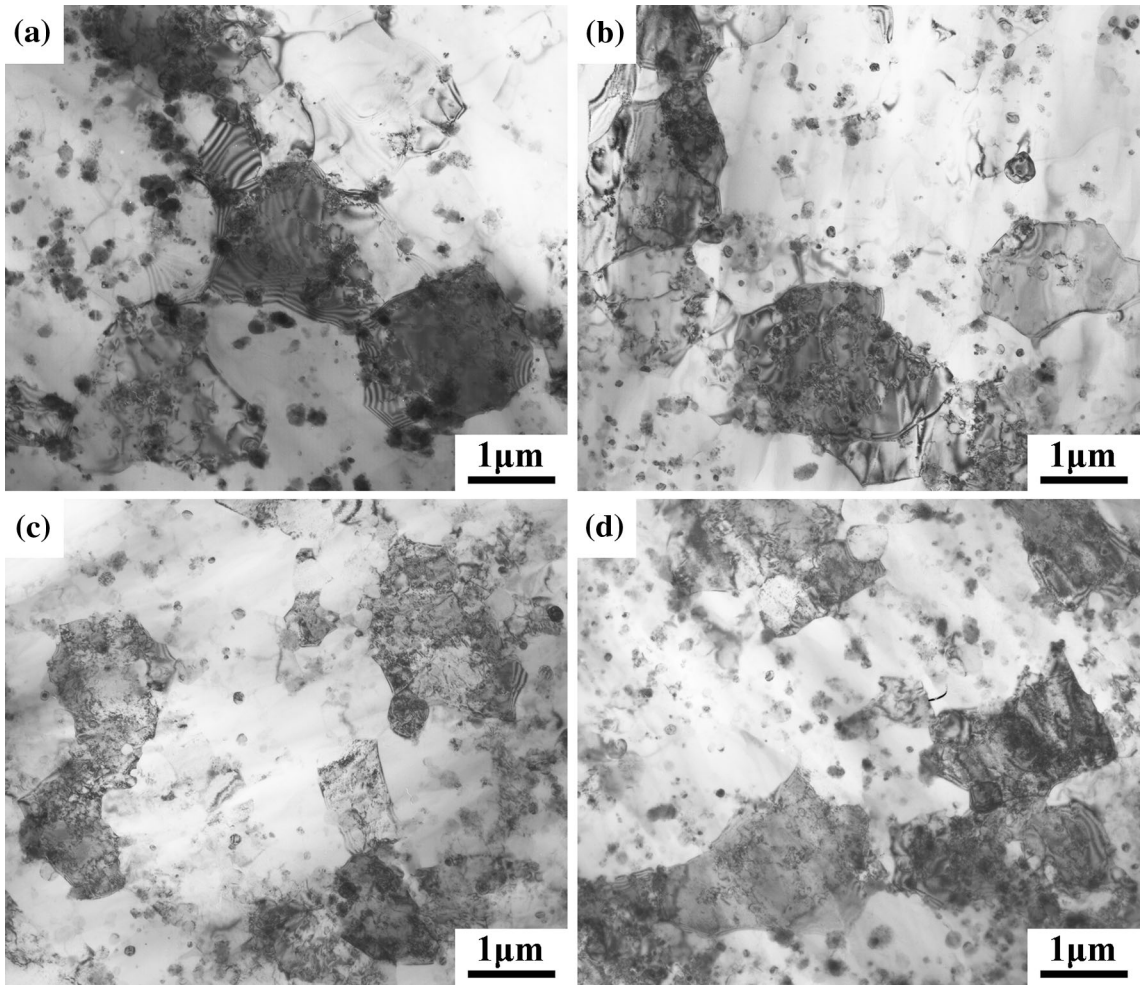

Fig. 11—TEM images of FSP samples 4 – 7 showing the grain microstructures in (*a*) sample 4, (*b*) sample 5, (*c*) sample 6, and (*d*) sample 7.

grain size exists undoubtedly for particle-reinforced metal matrix composites and was inversely proportional to f^n.

In the current study, Figure 10 shows that, at a traverse speed of 25 mm/min, increasing the tool rotation rate from 1000 to 2000 rpm caused little influence on the size and the number of Al_3Ti and Al_2O_3 particles, implying that the pinning effect of the particles on the grain boundaries did not change. However, Figure 11 shows that increasing the tool rotation rate from 1000 to 2000 rpm, which increased the heat input during FSP, still caused little influence on the grain size of the matrix. This may be attributed the two factors. First, a previous study[26] indicated that, although increasing the tool rotation rate would increase the peak temperature of the SZ during FSP, the temperature rise would become slow at the high rotation rate. For example, an investigation by Tang *et al.*[27] indicated that the peak temperature in the SZ increased by almost 313 K (40 °C) with increasing tool rotation rate from 300 to 650 rpm, whereas it only increased by 293 K (20 °C) when the tool rotation rate from 650 to 1000 rpm. Second, at a tool traverse speed of 25 mm/min and a rotation rate of 1000 rpm, the matrix grain size might have reached the limiting values during the thermal exposure caused by FSP and heat release of the *in situ* reaction. So increasing the tool rotation rate did not coarsen the matrix grains almost.

Figure 12 shows the EBSD microstructures of FSP sample 6. The average grain size of FSP sample 6 was determined to be 1.7 μm, which is consistent with the result of TEM (Figure 11(c)). The grain-boundary misorientation angle distribution of FSP sample 6 is shown in Figure 12(b). The fraction of high-angle grain boundaries (HAGBs, misorientation angle > 15 deg) was 92 pct, which was similar with that in the conventional FSP Al alloys.[28,29] Furthermore, it was revealed that FSP sample 6 exhibited a very weak texture component as indicated by the pole figures in Figure 12(c). These grain characteristics indicated that the fine equiaxed grains in FSP *in situ* composites resulted from dynamic recrystallization.[30] It is reported that, during FSP, the initial size of newly recrystallized grains near the pin was on the order of 25 – 100 nm.[31,32] During subsequent processing, the initial microstructures evolved due to the thermomechanical deformation behind the pin tool. The process included grain growth, introduction of additional dislocations, and recovery in the grains.[33] The grain size in FSP sample 6 was still

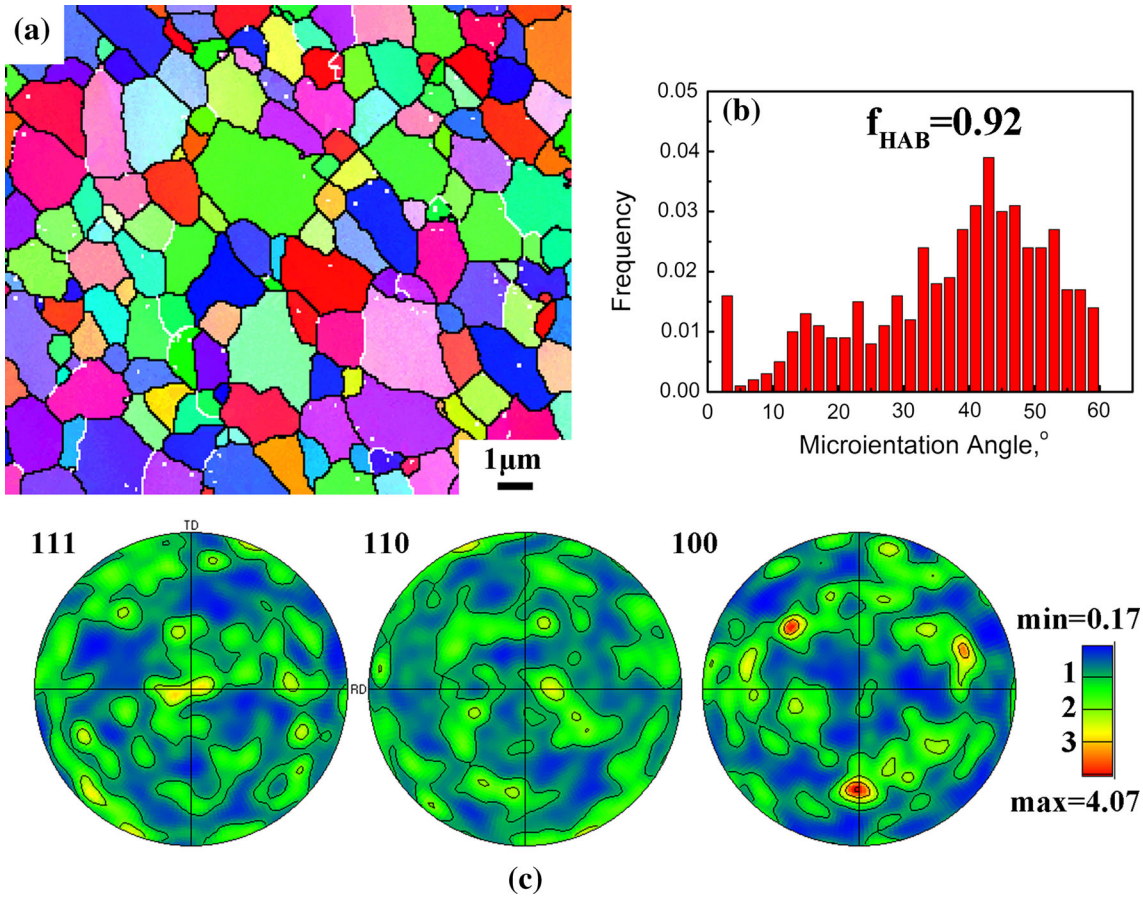

Fig. 12—EBSD microstructures of FSP sample 6: (*a*) EBSD orientation map, (*b*) grain-boundary misorientation angle distribution, and (*c*) pole figures.

smaller than that reported in most of FSW/FSP Al alloys[21–23] due to the inhibiting and pining effect of the Al_3Ti and Al_2O_3 particles on the growth of the grains.

Figure 13 shows the EBSD microstructures of FSP sample 8. The average grain size was determined to be 0.8 μm (Figure 13(a)). For sample 8, additional 2-pass FSP in water with a traverse speed of 50 mm/min was conducted after 4-pass FSP in air. The cooling rate during FSP in water increased significantly compared with that in air. Thus, the growth of the recrystallized grains was effectively inhibited, resulting in the ultrafine grains in FSP sample 8. Furthermore, previous studies[9,33] indicated that the high cooling rate during FSP would retain more dislocations in the grains. Figures 13(b) and (c) show that the matrix grain structure of FSP sample 8 still exhibited the characteristics of the high ratio of HAGBs and weak texture, indicating that the grain-refinement mechanism during FSP in water was still dynamic recrystallization.[34,35]

Figure 14 shows the reinforcing particles in FSP sample 8. It can be seen that the size and distribution of particles in FSP sample 8 were similar with those in FSP sample 6, suggesting that additional 2-pass FSP in water after 4-pass FSP in air exerted little influence on the *in situ* Al-TiO_2 reaction. First, after 4-pass FSP in air with a rotation rate of 1000 rpm and a traverse speed of 25 mm/min, most of TiO_2 had reacted with Al to form Al_3Ti and Al_2O_3. Second, additional 2-pass FSP were conducted in water and the traverse speed increased to 50 mm/min, so the peak temperature and duration of thermal exposure would be decreased significantly. Third, Al_3Ti and Al_2O_3 have the low coarsening rate below 873 K (600 °C).[15] Thus additional 2-pass FSP in water neither induced more Al-TiO_2 reaction nor coarsened Al_3Ti and Al_2O_3 particles.

B. *Tensile Properties*

Table II summarizes the tensile properties of various FSP samples. For comparison, the tensile properties of FSP pure Al reported in Reference 6 are listed in Table II. All the FSP samples exhibited the higher yield strength (YS) and ultimate tensile strength (UTS) compared with the FSP pure Al due to the presence of the reinforcing particles. Our previous study[6] suggested that the YS improvement of the *in situ* composites can be attributed to the Orowan strengthening and grain refinement caused by the *in situ* particles. However, the improvement of UTS would be attributed to not only Orowan strengthening and grain refinement but also higher strain hardening tendency caused by the *in situ* particles.[6]

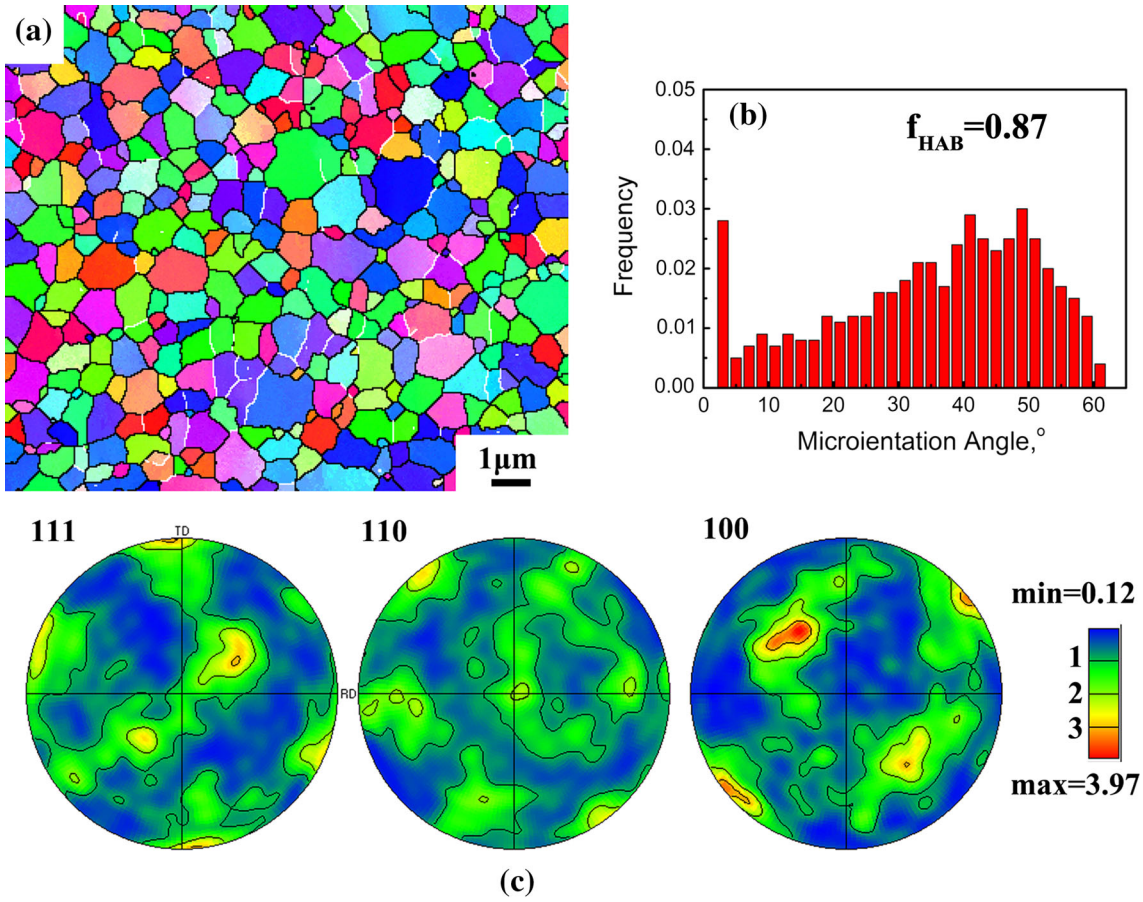

Fig. 13—EBSD microstructures of FSP sample 8: (*a*) EBSD orientation map, (*b*) grain-boundary misorientation angle distribution, and (*c*) pole figures.

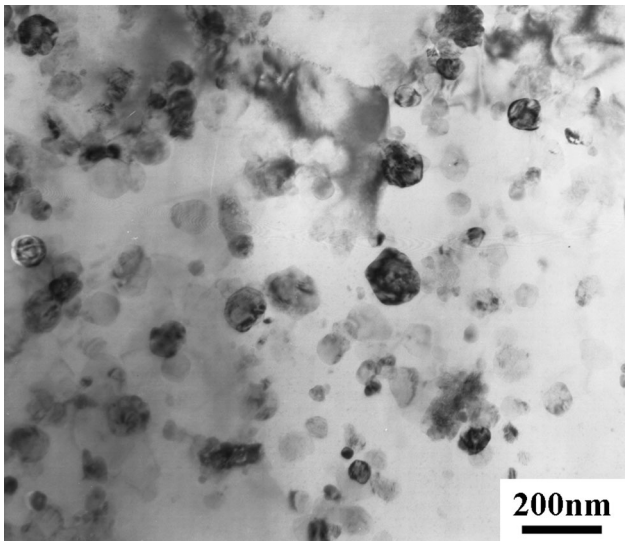

Fig. 14—TEM image of FSP sample 8 showing the reinforcing particles.

The enhancement of strain hardening of the *in situ* composites comes from two factors.[36–38] First, when a dislocation bypasses a particle, a dislocation loop would be remained around the particle, resulting in the enhancement of strain straining.[36] Second, during the deformation of *in situ* composites, the particles would constrain the deformation of matrix due to different elastic moduli of reinforcing particle and Al matrix, resulting in the formation of the "geometrically necessary" dislocations.[37,38] Thus the dislocation density in the matrix would increase, thereby enhancing strain hardening. When the reinforcing particle is smaller than 1 μm (such as Al_3Ti and Al_2O_3 in samples 1, 2, and 4 – 8), the former mechanism would be dominant, and when the reinforcing particle is larger than 1 μm (such as Al_3Ti in sample 3), the dominant mechanism would be the latter.[36,37]

Table II. Tensile Properties of FSP Samples

Sample No.	YS (MPa)	UTS (MPa)	Elongation (pct)
1	225 ± 6	310 ± 2	13.2 ± 1.6
2	220 ± 4	306 ± 3	12.5 ± 1.1
3	192 ± 3	271 ± 5	12.3 ± 1.4
4	182 ± 5	271 ± 7	12.3 ± 0.8
5	215 ± 7	298 ± 4	13.5 ± 0.6
6	225 ± 6	310 ± 2	13.2 ± 1.6
7	220 ± 4	308 ± 5	11.7 ± 0.7
8	298 ± 5	364 ± 6	5.8 ± 0.8
FSP pure Al[6]	69 ± 6	109 ± 3	25 ± 0.9

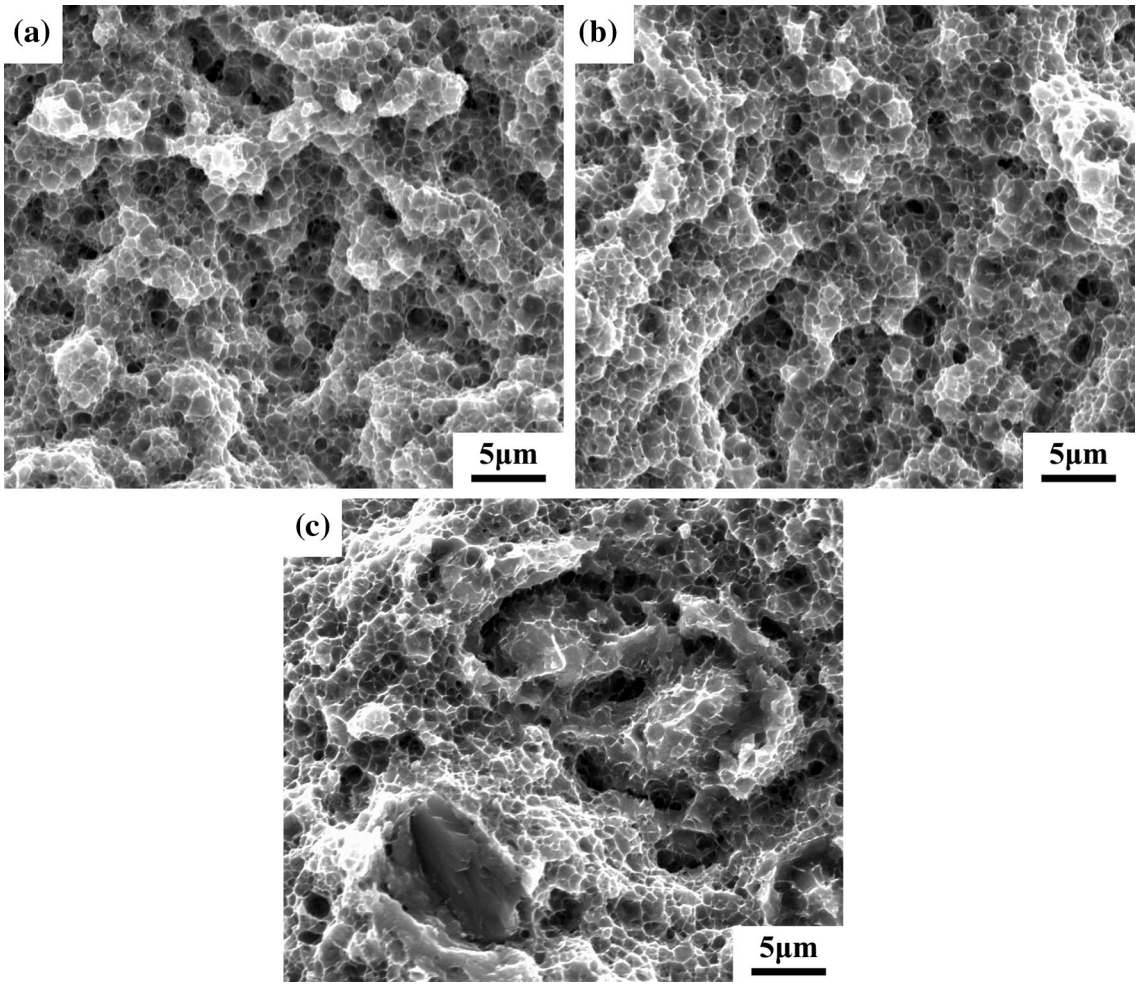

Fig. 15—SEM fractographs of FSP samples 1 – 3: (*a*) sample 1, (*b*) sample 2, and (*c*) sample 3.

FSP samples 1 and 2 exhibited almost the same tensile strength, whereas the YS and UTS of FSP sample 3 was reduced by about 30 MPa compared to those of FSP samples 1 and 2. Furthermore, the three samples exhibited similar elongations (12 to 13 pct).

Figure 15 shows the SEM micrographs of fracture surfaces of FSP samples 1 – 3. The fracture surfaces of the three samples all exhibited the characteristics of dimple fracture. For samples 1 and 2, the fine dimples with a narrow size distribution were observed (Figures 15(a) and (b)). For sample 3, except for some dimples, some cracked Al_3Ti particles were revealed (Figure 15(c)).

Samples 1 – 3 experienced different HP processes, resulting in different extents of Al-TiO_2 reaction during HP. For sample 1, the Al-TiO_2 reaction did not take place, whereas for sample 2, the Al-TiO_2 took place partly during HP. After FSP, some Al_3Ti and Al_2O_3 particles with a size of about 100 nm were formed in samples 1 and 2, and the number and distribution of the reinforcing particles were similar, yielding almost the same tensile properties and fracture patterns in both FSP samples 1 and 2. For sample 3, all TiO_2 reacted with Al to form Al_2O_3 with a size of about 150 nm and coarse Al_3Ti particles with a polygonal shape during HP. Although the edges and corners of most of polygonal Al_3Ti were rounded, creating some small Al_3Ti particles in the matrix, the Al_3Ti particles in FSP sample 3 were still relatively coarse. These coarse Al_3Ti tended to crack during tension, resulting in reduced strength. Once the particles cracked, the constraint of particle to the matrix deformation would be reduced, and then the density of "geometrically necessary" dislocations would not increase, weakening the strain hardening property.[36,37] So the strength of FSP sample 3 was lower than that of FSP samples 1 and 2, and some cracked Al_3Ti particles were observed on the fracture surface of FSP sample 3 (Figure 14(c)).

Furthermore, in the previous studies,[12,16] the *in situ* (Al_3Ti + Al_2O_3)/Al composites fabricated by HP, in which Al_3Ti particles were rod shaped with a large aspect ratio, usually exhibited lower elongations (≤ 5 pct), because the rod-shaped particles preferentially cracked at the low stress during tension. Compared with rod-shaped particles, the round Al_3Ti particles with a small aspect ratio would diminish the stress

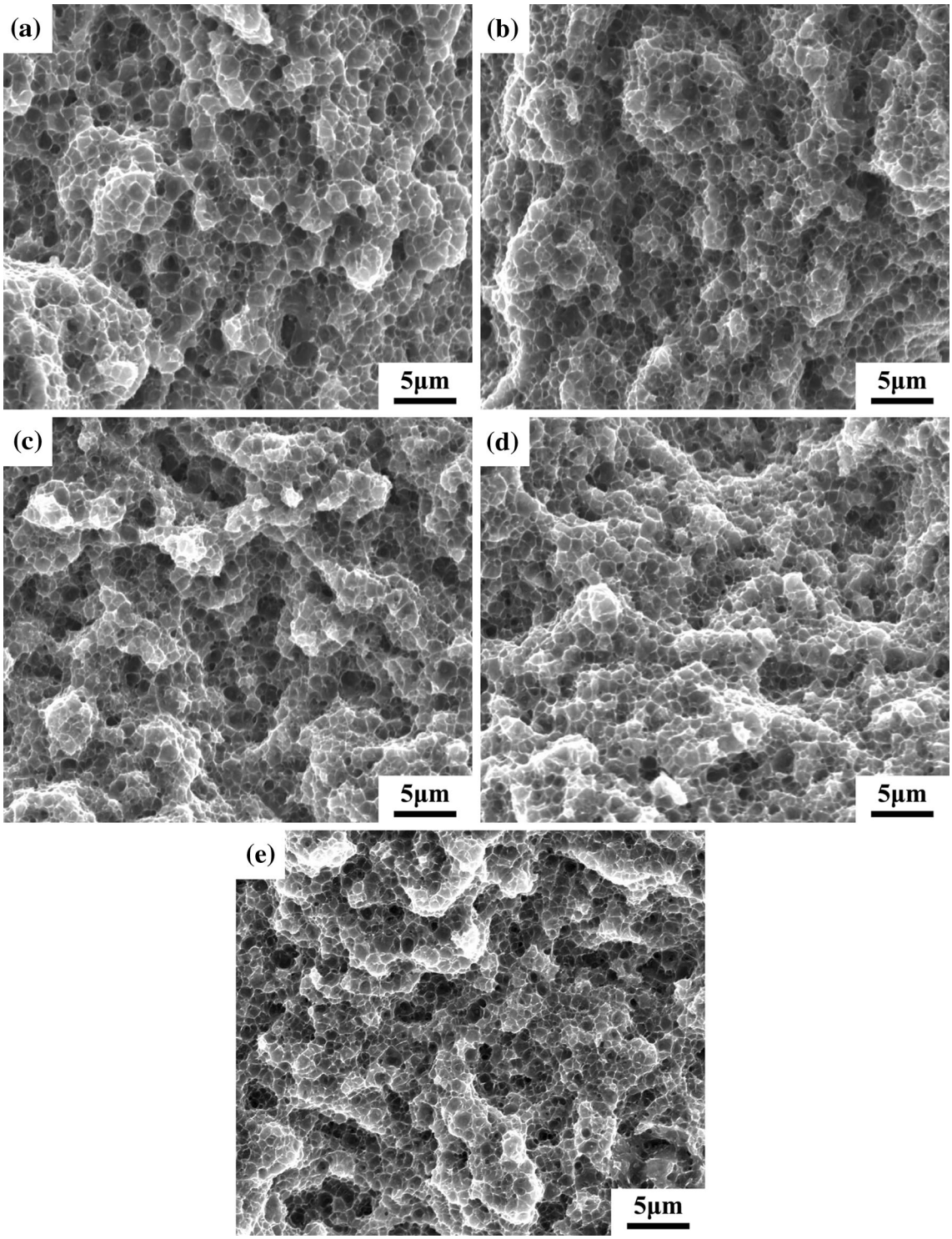

Fig. 16—SEM fractographs of FSP samples 4 – 8: (*a*) sample 4, (*b*) sample 5, (*c*) sample 6, (*d*) sample 7, and (*e*) sample 8.

concentration during tension. Therefore, FSP sample 3 still exhibited a comparable elongation with that of FSP samples 1 and 2.

The effects of FSP parameters on the tensile properties could be obtained from the comparison of the tensile properties of FSP samples 4 – 8. First, at a tool rotation rate of 1000 rpm, with decreasing the traverse speed from 100 to 25 mm/min, the YS and UTS of the FSP samples increased, whereas the elongation did not change almost. Second, at a traverse speed of 25 mm/min, increasing the tool rotation rate from 1000 to 2000 rpm caused no detectable influence on the tensile properties of the FSP samples. Third, the additional 2-pass FSP in water after 4-pass FSP in air increased the strength of the FSP samples significantly; however, it decreased the tensile elongation.

As shown in Figures 10 and 11, decreasing the traverse speed from 100 to 25 mm/min did not change the matrix grain size; however, it resulted in the decrease in the number of floc-shaped particles and the formation of more Al_3Ti and Al_2O_3. Because the size of Al_3Ti and Al_2O_3 was much smaller than that of floc-shaped particles,[6] the strengthening effect of reinforcing particles based on the Orowan mechanism[36] would increase with decreasing the traverse speed, leading to the increase in the tensile strength of the FSP samples. However, the elongation of FSP samples was independent of the traverse speed. The reasons for this were still not very clear. A possible reason is that the elongation was less sensitive to the microstructure change than YS and UTS of FSP *in situ* composites with homogeneous distribution of reinforcing particles.

At a traverse speed of 25 mm/min, increasing the tool rotation rate from 1000 to 2000 rpm caused little influence on the microstructures of the FSP samples, thereby causing little change to the tensile properties of the FSP samples. The increase in the tensile strength of the FSP samples after additional 2-pass FSP in water could be attributed to the following factors. First, the FSP in water refined the matrix grains significantly. Based on the Hall-Petch relationship, the strength would be increased due to grain boundary strengthening. Second, as discussed above, more dislocations would be retained in the matrix grains after FSP in water due to the rapid cooling,[9,32] which would increase the strength of the FSP samples further.

However, for the ultrafine grains with a high density of dislocations, the capability of accommodating dislocation would become poor during tension, resulting in the rapid plastic instability and the decrease in the tensile ductility.[38,39]

Figure 16 shows the SEM fractographs of FSP samples 4 – 8. The typical ductile dimple-fracture morphologies were observed in all the FSP samples. However, the dimple size of FSP sample 4 was slightly larger than that of other FSP samples. As presented in Figure 10, FSP sample 4 had fewer Al_3Ti and Al_2O_3 due to a higher traverse speed. The fewer Al_3Ti and Al_2O_3 resulted in the larger interparticle distance, thereby leading to the larger dimple size on the fracture surface.[40] This was consistent with the lower tensile strength of FSP sample 4. With decreasing the traverse speed of FSP, the number of nanosized Al_3Ti and Al_2O_3 increased, resulting in the decrease of the interparticle distance and the dimple size on the fracture surfaces.

Although additional 2-pass FSP in water refined the matrix grains, resulting in the increase in the tensile strength of the FSP sample, it caused little influence on the distribution and size of Al_3Ti and Al_2O_3 particles. So the size and morphology of the dimples on the fracture surface did not change. Similar results had been reported by Zhang *et al.*[9] in the FSP *in situ* Al_3Ti/Al composites.

IV. CONCLUSIONS

The effects of HP and FSP parameters on the microstructures and mechanical properties of *in situ* composites based on the Al-TiO_2 system were studied in the present study and the following conclusions can be reached:

1. The Al-TiO_2 reaction hardly took place during HP at 773 K (500 °C) with a holding time of 5 minutes. The Al-TiO_2 reaction took place partly during HP at 823 K (550 °C) with a holding time of 50 minutes. All the TiO_2 reacted with Al to form coarse and polygonal Al_3Ti particles and Al_2O_3 particles with a size of 150 nm during HP at 903 K (630 °C) with a holding time of 240 minutes.
2. For samples in which the Al-TiO_2 reaction took place hardly or partly, subsequent FSP induced the Al-TiO_2 reaction, resulting in the formation of Al_3Ti and Al_2O_3 with a size of about 100 nm. For the sample in which the Al-TiO_2 reaction took place completely during HP, subsequent FSP blunted the polygonal Al_3Ti particles and distributed the Al_2O_3 homogeneously in the matrix. The tensile strength of the FSP sample in which the Al-TiO_2 reaction took place completely during HP was lower than that of FSP samples in which the Al-TiO_2 reaction took place hardly or partly during HP.
3. For the FSP sample in which the Al-TiO_2 reaction did not take place during HP, the volume fraction of reinforcing particles increased with decreasing the traverse speed; however, the matrix grain size was not influenced by the traverse speed of FSP. Thus, the strength of the FSP samples increased as the traverse speed of FSP decreased. When the traverse speed was 25 mm/min, increasing tool rotation rate from 1000 to 2000 rpm caused little influence on the microstructure and mechanical properties of the *in situ* composites.
4. Additional 2-pass FSP in water did not change the size and distribution of reinforcing particles, but it refined the matrix grains, resulting in the increase in the tensile strength and the decrease in the elongation of the *in situ* composite.

ACKNOWLEDGMENTS

The authors gratefully acknowledge the support of the National Natural Science Foundation of China under No. 51331008.

REFERENCES

1. R.S. Mishra, M.W. Mahoney, S.X. McFadden, N.A. Mara, and A.K. Mukherjee: *Scripta Mater.*, 2000, vol. 42, pp. 163–68.
2. C.J. Hsu, C.Y. Chang, P.K. Kao, N.J. Ho, and C.P. Chang: *Acta Mater.*, 2006, vol. 54, pp. 5241–49.
3. C.J. Hsu, P.W. Kao, and N.J. Ho: *Scripta Mater.*, 2005, vol. 53, pp. 341–45.
4. Q. Zhang, B.L. Xiao, Q.Z. Wang, and Z.Y. Ma: *Mater. Lett.*, 2011, vol. 65, pp. 2070–72.
5. Q. Zhang, B.L. Xiao, and Z.Y. Ma: *Mater. Chem. Phys.*, 2013, vol. 139, pp. 596–602.
6. Q. Zhang, B.L. Xiao, W.G. Wang, and Z.Y. Ma: *Acta Mater.*, 2012, vol. 60, pp. 7090–7103.

7. Q. Zhang, B.L. Xiao, D. Wang, and Z.Y. Ma: *Mater. Chem. Phys.*, 2011, vol. 130, pp. 1109–17.
8. C.F. Chen, P.W. Kao, L.W. Chang, and N.J. Ho: *Metall. Mater. Trans. A*, 2010, vol. 41A, pp. 513–22.
9. Q. Zhang, B.L. Xiao, P. Xue, and Z.Y. Ma: *Mater. Chem. Phys.*, 2012, vol. 134, pp. 294–301.
10. Z.Y. Liu, Q.Z. Wang, B.L. Xiao, Z.Y. Ma, and Y. Liu: *Mater. Sci. Eng. A*, 2010, vol. 527, pp. 5582–91.
11. G.B. Schaffer and P.G. McCormick: *Metall. Trans. A*, 1990, vol. 21A, pp. 2789–94.
12. Z.Y. Ma and S.C. Tjong: *Metall. Mater. Trans. A*, 1997, vol. 28A, pp. 1931–42.
13. C.F. Feng and L. Froyen: *Composite A*, 2000, vol. 31, pp. 385–90.
14. C.F. Feng and L. Froyen: *Scripta Mater.*, 1998, vol. 39, pp. 109–18.
15. S.H. Wang and P.W. Kao: *Acta Mater.*, 1998, vol. 46, pp. 2675–82.
16. H.G. Zhu, H.Z. Wang, L.Q. Ge, W.J. Xu, and Y.Z. Yuan: *Mater. Sci. Eng. A*, 2008, vol. 478, pp. 87–92.
17. Z.Y. Ma, S.R. Sharma, and R.S. Mishra: *Metall. Mater. Trans. A*, 2006, vol. 37A, pp. 3323–36.
18. A.H. Feng, B.L. Xiao, and Z.Y. Ma: *Compos. Sci. Technol.*, 2008, vol. 68, pp. 2141–48.
19. L.M. Marzoli, A.V. Strombeck, J.F. Dos Santos, C. Gambaro, and L.M. Volpone: *Compos. Sci. Technol.*, 2006, vol. 66, pp. 363–71.
20. G.L. You, N.J. Ho, and P.W. Kao: *Mater. Charact.*, 2013, vol. 80, pp. 1–8.
21. R.S. Mishra and Z.Y. Ma: *Mater. Sci. Eng. R.*, 2005, vol. R50, pp. 1–78.
22. Y.S. Sato, S.H.C. Park, and H. Kokawa: *Metall. Mater. Trans. A*, 2001, vol. 32A, pp. 3023–31.
23. H.G. Salem, A.P. Reynolds, and J.S. Lyons: *Scripta Mater.*, 2002, vol. 46, pp. 337–42.
24. F.J. Humphreys and M. Hatherly: *Recrystallization and Related Annealing Phenomena*, 2nd ed., Elsevier Ltd., Amsterdam, The Netherlands, 2004.
25. Z.Y. Ma, S.R. Sharma, and R.S. Mishra: *Mater. Sci. Eng. A*, 2006, vol. 433, pp. 269–78.
26. N. Maazi and N. Rouag: *J. Cryst. Growth*, 2002, vol. 243, pp. 361–69.
27. W. Tang, X. Guo, J.C. McClure, and L.E. Murr: *J. Mater. Process. Manufact. Sci.*, 1998, vol. 7, pp. 163–72.
28. Y.S. Sato, M. Urata, and H. Kokawa: *Metall. Mater. Trans. A*, 2002, vol. 33A, pp. 625–35.
29. F.C. Liu, Z.Y. Ma, and L.Q. Chen: *Scripta Mater.*, 2009, vol. 60, pp. 96–971.
30. I. Charit and R.S. Mishra: *Mater. Sci. Eng. A*, 2003, vol. 359, pp. 290–96.
31. Z.Y. Ma: *Metall. Mater. Trans. A*, 2008, vol. 39A, pp. 642–58.
32. C.G. Rhodes, M.W. Mahoney, W.H. Bingel, and M. Calabrese: *Scripta Mater.*, 2003, vol. 48, pp. 1451–55.
33. R.W. Fonda, J.F. Bingert, and K.J. Colligan: *Scripta Mater.*, 2004, vol. 51, pp. 243–48.
34. J.Q. Su, T.W. Nelson, and C.J. Sterling: *Scripta Mater.*, 2005, vol. 52, pp. 135–40.
35. J.Q. Su, T.W. Nelson, T.R. McNelley, and R.S. Mishra: *Mater. Sci. Eng. A*, 2011, vol. 528, pp. 5458–64.
36. J.W. Martin: *Micromechanisms in Particle Hardened Alloys*, Cambridge University Press, Cambridge, U.K., 1980.
37. T.S. Srivatsan, A.H. Meslet, C. Smith, and M. Petraroli: *Mater. Sci. Eng. A*, 2003, vol. 346, pp. 91–100.
38. Y.H. Zhao, Y.T. Zhu, and E.J. Lavernia: *Adv. Eng. Mater.*, 2010, vol. 12, pp. 769–78.
39. X.H. An, Q.Y. Lin, S.D. Wu, Z.F. Zhang, R.B. Figueiredo, N. Gao, and T.G. Langdon: *Scripta Mater.*, 2011, vol. 64, pp. 954–57.
40. Y.C. Kang and S.L. Chan: *Mater. Chem. Phys.*, 2004, vol. 85, pp. 438–43.